

Modeling the Fermi arc in underdoped cuprates

M. R. Norman,¹ A. Kanigel,² M. Randeria,³ U. Chatterjee,² and J. C. Campuzano^{2,1}

¹Materials Science Division, Argonne National Laboratory, Argonne, IL 60439

²Department of Physics, University of Illinois at Chicago, Chicago, IL 60607

³Department of Physics, The Ohio State University, Columbus, OH 43210

(Dated: November 18, 2021)

Angle resolved photoemission data in the pseudogap phase of underdoped cuprates have revealed the presence of a truncated Fermi surface consisting of Fermi arcs. We compare a number of proposed models for the arcs, and find that the one that best models the data is a d-wave energy gap with a lifetime broadening whose temperature dependence is suggestive of fluctuating pairs.

PACS numbers: 74.25.Jb, 74.72.Hs, 79.60.Bm

I. INTRODUCTION

It is well established that cuprates possess a superconducting phase with an order parameter that has d-wave symmetry,¹ and for hole-doped materials, this phase exists over a range of doping above 5%. It is also well established that at very low dopings, the material is an antiferromagnetic Mott insulator. Connecting these two states is an unusual phase known as the pseudogap, the nature of which is still being debated.² It is felt by many that the proper identification of this phase will have a major impact on the ultimate ‘mechanism’ for pairing in cuprate superconductors.

Angle resolved photoemission spectroscopy (ARPES) reveals the presence of a truncated Fermi surface in the pseudogap phase.^{3,4,5} In a study of the pseudogap versus temperature,⁶ this truncated Fermi surface was denoted as a ‘Fermi arc’. The arc was shown to be intermediate between the d-wave node of the superconductor and the complete Fermi surface of the normal state. Moreover, the arc appears to form by a closing of the energy gap of the superconducting state as the temperature is raised above T_c . Off the arc, in the ‘pseudogapped’ (antinode) region of the Brillouin zone, the spectral gap appears instead to fill in with temperature. This filling in effect is also seen in c-axis conductivity data⁷ and is consistent with the thermal evolution of the specific heat.⁸ This ‘dual’ nature of the energy gap is suggestive of a ‘two gap’ scenario where a ‘superconducting’ gap resides on the arc and a ‘pseudogap’ resides off the arc. Such a two gap picture was proposed by Deutscher,⁹ and recent Raman,¹⁰ ARPES,^{11,12} and STM¹³ data have been offered in its support. On the other hand, even for underdoped samples, the gap function below T_c seems to be more or less d-wave like.¹⁴ This conundrum of having a single gap below T_c transforming into a dual gap above T_c was stressed sometime ago.¹⁵

Recently, a very detailed temperature and doping study of the energy gap above T_c was done by Kanigel *et al.*¹⁶ They found that the length of the arc scales as T/T^* , where T^* , the temperature at which the spectral gap ‘fills up’ in the antinodal region of the zone, strongly increases with underdoping.¹⁷ As a consequence, the an-

gular anisotropy of the pseudogap looks more and more like a d-wave gap as the temperature is lowered relative to T^* . This finding is supported by thermal conductivity data, which indicates that the d-wave dispersion of the superconducting state at low temperatures survives when the doping is reduced into the pseudogap state.¹⁸ It is also consistent with recent ARPES and STM data on the stripe ordered phase of $\text{La}_{7/8}\text{Ba}_{1/8}\text{CuO}_4$, which indicates a d-wave like gap anisotropy at low temperatures (but above T_c).¹⁹ More recently, the study of Kanigel *et al.* has been extended to below T_c ,²⁰ where it was found that the arc collapses to a node within the resistive width of the transition, with a simple d-wave like gap below T_c . These recent studies bring into question the ‘two gap’ picture.

Primarily motivated by the ARPES data, a wide range of models have been proposed to explain the Fermi arc. Basically, these models can be grouped into two categories. In the first, the pseudogap is associated with a $q=0$ instability. Most of the models in this category have the pseudogap as a precursor to the superconducting gap, and involve pair formation with the absence of long range phase order.^{21,22,23} These models have been extended to describe the arc by explicitly invoking vortex-like excitations^{24,25,26,27} as revealed by measurements of the Nernst effect.²⁸ The node of the d-wave dispersion is broadened into an arc by a combination of lifetime broadening as well as Doppler shifts of the single particle states due to the vortices. There are, though, $q=0$ theories which do not involve superconductivity. One example is the model of Varma and Zhu,²⁹ which involves circulating currents within a CuO_2 plaquette (and thus has the same periodicity as the unit cell). In this case, the gap function has a ‘ d^2 ’ anisotropy. Another example is the ‘nodal nematic’ phase of Kim *et al.*,³⁰ where the node is displaced by a nematic order parameter rather than a vortex Doppler shift. The final example we mention is the model of Wen and Lee³¹ where the node is displaced in energy due to staggered flux phase correlations. In fact, a rich variety of behavior has been predicted within the general context of resonating valence bond (RVB) theories.^{32,33,34,35}

The second category involves a non-zero q vector. This

category ranges from models based on a precursor spin density wave,^{36,37} charge density wave,³⁸ stripes,³⁹ flux phases,³² or orbital currents.⁴⁰ In the case of fluctuating order,^{32,41,42,43} the non-zero q vector is not as obvious in the excitation spectrum. Those scenarios involving a (π, π) wavevector possess small hole pockets centered at $(\pi/2, \pi/2)$ where the intensity is reduced on one side of the pocket due to the amplitude factors which mix the states differing by q . Related models are those where the Luttinger surface (surface of zeros of the single particle Greens function) differs from the Fermi surface.^{44,45,46,47} In this case, the Fermi surface is truncated where it crosses the Luttinger surface. In a more general $2k_F$ context, the flat parts of the Fermi surface which reside in the antinodal region of the zone can be eliminated by nesting,^{48,49} leaving a residual arc.

In this paper, some of these scenarios will be addressed in the context of the ARPES data. In Section II, several non-zero q scenarios, where for simplicity long range order is assumed, will be analyzed. These scenarios typically lead to (a) Fermi arcs whose length is T independent, (b) deviations of the arcs from the underlying Fermi surface, (c) energy gaps which are not centered symmetrically about the Fermi energy, and (d) shadow bands. We argue that there is no evidence for these effects in ARPES and tunneling data, at least in the mildly underdoped region. In Section III, we turn to the $q=0$ solutions. We find that the scenario most consistent with the data is one where the node remains along the zone diagonal and at the Fermi energy. The temperature evolution of the arc above T_c is consistent with lifetime broadening of the node, though the data also indicate a distortion of the d-wave gap anisotropy with temperature. In Section IV, we offer some conclusions, and suggest future ARPES experiments that could further differentiate between the various models for the Fermi arc.

II. NON ZERO Q SCENARIOS

A. Commensurate density wave

These scenarios assume a q vector of (π, π) with an energy gap that is either isotropic, or has d-wave symmetry.⁴⁰ The secular matrix is of 2 by 2 form, and the Greens function associated with the wavevector k in the presence of simple elastic broadening, Γ , can be written as:

$$G_k = \left(\frac{E_+ - \epsilon_{k+q}}{E_+ - E_-} \right) \frac{1}{\omega - E_+ + i\Gamma} - \left(\frac{E_- - \epsilon_{k+q}}{E_+ - E_-} \right) \frac{1}{\omega - E_- + i\Gamma} \quad (1)$$

where

$$E_{\pm} = \frac{\epsilon_k + \epsilon_{k+q}}{2} \pm \sqrt{\left(\frac{\epsilon_k - \epsilon_{k+q}}{2} \right)^2 + \Delta_k^2} \quad (2)$$

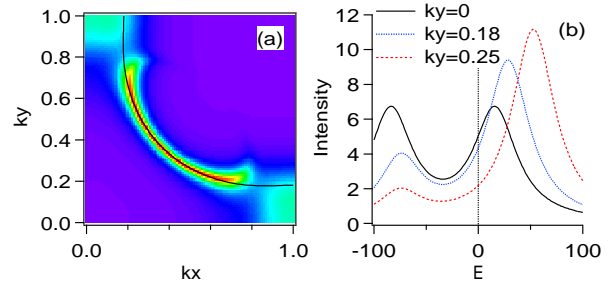


FIG. 1: (Color online) (a) Spectral intensity at zero energy versus k_x, k_y , and (b) versus energy for $k_x = 1$ for several k_y , for the d-density wave model.⁴⁰ The black curve in (a) is the normal state Fermi surface. Zone dimensions for all figures are in π/a units, and energies are in meV. For all figures (unless otherwise noted), $\Delta_0=50$ meV and $\Gamma=25$ meV.

We have looked at several cases, with various dispersions, ϵ_k , including some with bilayer splitting, and several different forms for Δ_k . For brevity, we present results using for ϵ_k the tight binding dispersion of Norman *et al.*⁵⁰ and a d-density wave gap⁴⁰ $\Delta_k = \frac{\Delta_0}{2}(\cos(k_x) - \cos(k_y))$.

In Fig. 1a, we present the intensity plot of the spectral function (imaginary part of G_k) in the 2D zone for $\omega = 0$. At the simplest level, one indeed finds an arc. But there are several details worth pointing out. First, the ends of the arc turn away from the underlying Fermi surface of the normal state. This is due to the fact that the zero energy contour traces out a pocket centered at $(\pi/2, \pi/2)$, the back side of which is suppressed by the coherence factors (the prefactor of each term in Eq. 1). Second, there is a strong suppression of the intensity at the ‘hot spots’ - the points where the normal state Fermi surface ($\epsilon_k = 0$) crosses its (π, π) displaced image. This can be related to the ‘Luttinger surface’ effect mentioned in the Introduction. To see this, we note that the Greens function in this model can be rewritten as:

$$G_k^{-1} = \omega - \epsilon_k + i\Gamma - \frac{\Delta_k^2}{\omega - \epsilon_{k+q} + i\Gamma} \quad (3)$$

The ‘gap’ self-energy (the last term of this equation) diverges when $\omega = \epsilon_{k+q}$ in the absence of broadening ($\Gamma = 0$). Thus the (π, π) translated image of the normal state Fermi surface ($\epsilon_{k+q} = 0$) is the Luttinger surface, and therefore the zero energy intensity is suppressed when the normal state Fermi surface crosses this surface. Finally, there is weaker intensity centered around the $(\pi, 0)$ points which will be suppressed as Δ_0 increases. To investigate this further, in Fig. 1b, we show the spectral function for several k points along the $(\pi, 0) - (\pi, \pi)$ direction. One clearly sees that the spectral function has a minimum value that sits at negative energy. At $k = (\pi, 0)$, it is obvious from Eq. 2 that this minimum value occurs at $\omega = \epsilon_k$, which is -34 meV for this dispersion. This asymmetry in energy is obviously enhanced for dispersions where $\epsilon_{\pi,0}$ is deeper in energy.

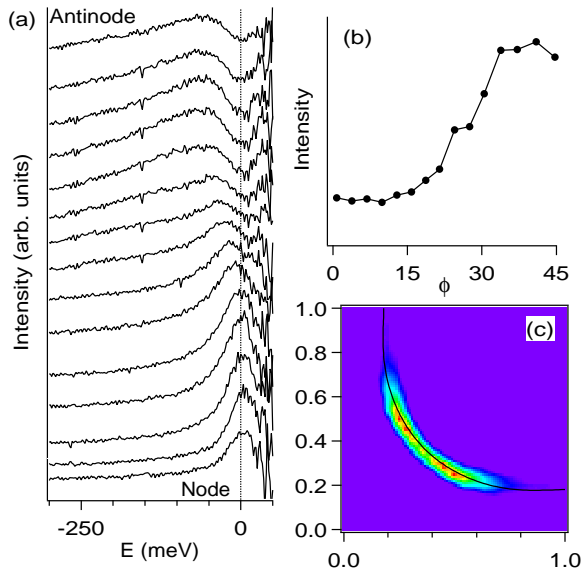


FIG. 2: (Color online) (a) Experimental energy distribution curves (EDCs) for optimal doped $\text{Bi}_2\text{Sr}_2\text{CaCu}_2\text{O}_8$ (Bi2212) around the underlying Fermi surface in the pseudogap phase ($T=140\text{K}$) divided by a resolution broadened Fermi function. The bottom curve is at the node and the top curve at the antinode. The data set is the same as in Fig. 1b of Ref. 16. (b) Zero energy intensity from (a) as a function of the Fermi surface angle, ϕ , where $\phi = 0^\circ$ corresponds to the antinode and $\phi = 45^\circ$ to the node. (c) Zero energy intensity versus k_x, k_y (the data were reflected relative to $k_x = k_y$). For (b), the intensities were obtained by subtracting a background EDC (obtained from an unoccupied k), then normalizing this subtracted intensity by its energy integrated weight. This was designed to minimize the effect of the photoemission matrix elements. This was not done in (c) in order to demonstrate that the raw data show no indication for any deviation of the arc from the underlying Fermi surface (black curve).

In relation to the experimental data, we note the following issues with this model, which are generic to models based on a finite q order parameter. First, there is no natural way to generate an arc whose length is proportional to the temperature. Second, there is no evidence from ARPES for a ‘turn in’ of the ends of the arc away from the underlying normal state Fermi surface (Fig. 2c). Third, ARPES is consistent with spectral functions which either have a maximum (arc) or minimum (antinode region) at zero energy along the underlying Fermi surface. We demonstrate this in Fig. 2a, where data in the pseudogap phase along the underlying Fermi surface is plotted. These data are the same as used to construct Fig. 1b of Ref. 16, but instead of ‘symmetrizing’ the raw data as was done there (which implicitly assumes a maximum or minimum at zero energy), we divide the data by a resolution broadened Fermi function. The clear maxima at zero energy along the arc, and the minima at zero energy away from the arc, are quite ev-

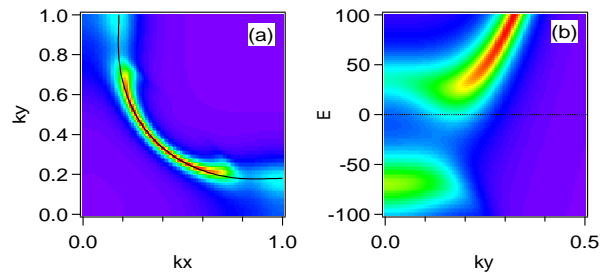


FIG. 3: (Color online) (a) Spectral intensity at zero energy versus k_x, k_y , and (b) versus energy and k_y for $k_x = 1$, for the model of Yang *et al.*⁴⁴

ident. This is consistent with tunneling data as well⁵¹ where the minimum in the tunneling conductance is at zero bias, even in the pseudogap phase.

B. Differing Luttinger surface

These scenarios^{44,45,46,47} are related to the ones just discussed. For discussion purposes, we look at the recently proposed model of Yang, Rice, and Zhang.⁴⁴ In this case, the Greens function is

$$G_k^{-1} = \omega - \epsilon_k + i\Gamma - \frac{\Delta_k^2}{\omega + \epsilon_k^{NN} + i\Gamma} \quad (4)$$

where ϵ_k^{NN} is just the near neighbor term of the tight binding dispersion (Δ_k has the same form as the d density-wave case). Note that if ϵ_k only had a near neighbor term, then at half filling, this model would be equivalent to the d density-wave model. The similarity of these two models can be seen in Fig. 3, where we show the zero energy intensity plot in the 2D zone, as well as the intensity versus ω for k along $(\pi, 0) - (\pi, \pi)$. Again, note the pronounced suppression of the intensity at the ‘hot spots’ in Fig. 3a, which is not evident in the data (a plot of the experimental zero energy intensity around the Fermi energy is shown in Fig. 2b), as well as the pronounced asymmetry of the energy gap relative to the Fermi energy in Fig. 3b. And, as with the d density-wave model, there is no obvious mechanism to obtain an arc proportional to T .

C. Nesting density wave

These scenarios assume a q vector which nests the antinodal points of the 2D Fermi surface. Two approximations were analyzed. In the first, a single q vector along q_y , $q = (0, -q)$, was used in the first octant (bounded by $(0, 0) - (\pi, 0) - (\pi, \pi) - (0, 0)$) of the square lattice zone (a 2 by 2 secular equation), the result of which was then reflected to the other octant. The orientation of q was designed so as to connect the antinode at

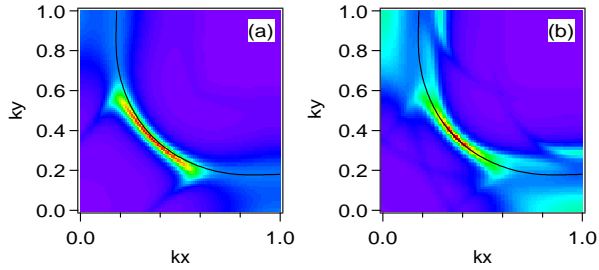


FIG. 4: (Color online) (a) Spectral intensity at zero energy versus k_x, k_y for (a) the 2 by 2 secular equation and (b) the 3 by 3 secular equation approximations, for the antinodal nesting model with $q = (0.36, 0)$.

$(\pi, q/2)$ with the one at $(\pi, -q/2)$. The equation for the Greens function is the same as in Eqs. 1 and 2, except that Δ_k in this case was taken to be isotropic.

In the second approximation, a 3 by 3 secular equation is separately solved for q vectors oriented respectively along q_x , $q = (q, 0)$ and $q = (-q, 0)$, and along q_y , $q = (0, q)$ and $q = (0, -q)$, in the first quadrant of the zone, and then the two results are averaged (representing averaging over two domains). The unaveraged G_k is given by

$$G_k = \sum_{i=1}^3 \frac{(E_i - \epsilon_{k+q})(E_i - \epsilon_{k-q})}{(E_i - E_{i+1})(E_i - E_{i+2})} \frac{1}{\omega - E_i + i\Gamma} \quad (5)$$

where by $i+1$ and $i+2$ we mean modulo 3. The E_i are given by solving the appropriate cubic equation and can be written as

$$E_i = -2\sqrt{d} \cos((\theta + 2\pi i)/3) - a/3 \quad (6)$$

where

$$\begin{aligned} a &= -(\epsilon_k + \epsilon_{k+q} + \epsilon_{k-q}) \\ b &= \epsilon_k \epsilon_{k+q} + \epsilon_k \epsilon_{k-q} + \epsilon_{k+q} \epsilon_{k-q} - 2\Delta_k^2 \\ c &= -\epsilon_k \epsilon_{k+q} \epsilon_{k-q} + \Delta_k^2 (\epsilon_{k+q} + \epsilon_{k-q}) \\ d &= (a^2 - 3b)/9 \\ r &= (2a^3 - 9ab + 27c)/54 \\ \theta &= \cos^{-1}(r/d^{3/2}) \end{aligned} \quad (7)$$

In Fig. 4, we show the zero energy intensity in the 2D zone for the two approximations. Again, a clear arc is seen, with extra structure that can be attributed to the reduced intensity (due again to the coherence factors) of the ‘shadow’ bands. This is particularly true in 4b where more shadow bands occur. A similar situation would occur if one had ‘checkerboard’ order (this would be obtained by solving a 5 by 5 secular matrix associated with a ‘double q ’ structure).

A significant difference from the previous cases is the origin of the arc. In the previous cases, the arc is due to the Fermi energy cutting across the lower of the two energy bands. In essence, the energy gap is centered above

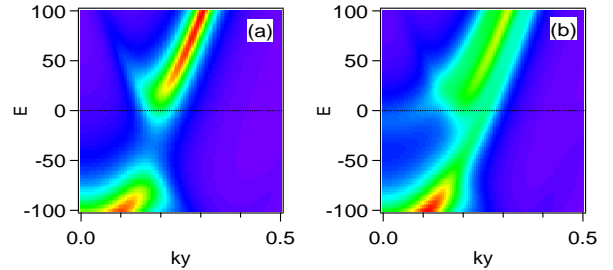


FIG. 5: (Color online) (a) Spectral intensity versus energy and k_y near the arc tip ($k_x = 0.6$) for (a) the 2 by 2 secular equation and (b) the 3 by 3 secular equation approximations, for the antinodal nesting model with $q = (0.36, 0)$.

the Fermi energy for k vectors from the node to the ‘hot spots’, and it is centered below the Fermi energy for k vectors from the ‘hot spots’ to the antinode. But in this ‘antinodal’ nesting case, it is the reverse situation. In the 2 by 2 approximation, the arc is formed from the Fermi energy cutting across the upper of the two bands. This is particularly evident near the arc tip, as shown in Fig. 5. In essence, the energy gap is centered below the Fermi energy for k along the arc. For momenta near the arc tip, one would find a minimum in the spectral function at a negative energy (as in Fig. 1b). This effect is not evident, though, in the ARPES data. And again, as the arc tip is associated with where the underlying normal state Fermi surface intersects the density wave zone boundary (in the first octant, this would correspond to $k_y = q/2$), there is no natural mechanism to arc proportional to temperature. As discussed by McElroy,⁴⁹ this would require a ‘two gap’ scenario, where the density wave gap would wipe out the antinodal parts of the Fermi surface, and then a second gap would wipe out the remaining arc with reducing temperature. Despite the attractiveness of such scenarios in regards to some experimental data,^{9,10,11,12,13} a definitive signature of this density wave gap would be to observe the shadow bands evident in Fig. 4 and the asymmetry of the gap relative to the Fermi energy evident in Fig. 5. So far, we have found no evidence for either of these effects.⁵²

III. ZERO Q SCENARIOS

A. Energy displaced node

The RVB model of Wen and Lee³¹ is based on incorporating both the effect of a d-wave gap in the particle-particle channel and a staggered flux phase gap in the particle-hole channel. An ansatz for the Greens function in this model that makes it of the same form as the earlier cases we studied is

$$G_k^{-1} = \omega - \epsilon_k + i\Gamma - \frac{\Delta_k^2}{\omega + \epsilon_k + \mu_{sh} + i\Gamma} \quad (8)$$

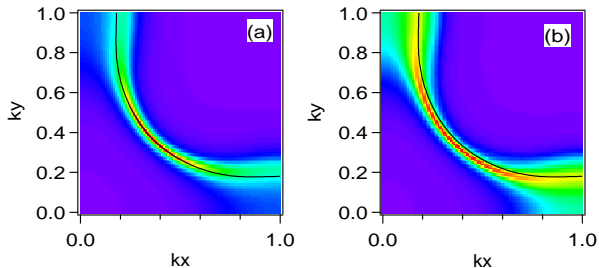


FIG. 6: (Color online) (a) Spectral intensity at (a) zero energy and (b) -25 meV versus k_x, k_y for the model of Wen and Lee with $\mu_{sh} = -50 \text{ meV}$.³¹

The effect of μ_{sh} is to move the d-wave node off the Fermi energy, and the sign of μ_{sh} is chosen to be negative so that the node is above the Fermi energy. The result is an arc at zero energy that is tied to the underlying Fermi surface (Fig. 6a). This is a positive feature of this model. If $|\mu_{sh}|$ were proportional to T for some (unknown) reason, this could also account for the temperature evolution of the arc. The major problem with this model, though, is that as one goes to positive energy, the arc would shrink in size, and as one goes to negative energy, the arc would expand in size. This effect is not evident in the ARPES data in the pseudogap phase, though, which seems to be more or less consistent with arcs which are independent of energy up to energy scales of order Δ_0 .⁵³ And in this model, the energy gap is always centered at an energy above the Fermi energy for all momentum cuts in the zone, an effect not visible in Fig. 2a.

B. d-wave pairs plus lifetime broadening

The simplest model in this class is equivalent to the one just described with $\mu_{sh} = 0$

$$G_k^{-1} = \omega - \epsilon_k + i\Gamma - \frac{\Delta_k^2}{\omega + \epsilon_k + i\Gamma}, \quad (9)$$

The spectral function for finite Γ traces out an ‘arc’, as shown in Fig. 7a. And the energy gap is centered at the Fermi energy, as shown in Fig. 7b. That is, the gap is tied to the Fermi energy and the Fermi surface, consistent with experiment. In Fig. 8a, we plot the evolution of the spectral function on the Fermi surface ($\epsilon_k = 0$) for this model, and in Fig. 8b the angular anisotropy of the spectral gap (half the peak to peak separation).

Gapped and ungapped spectra on the Fermi surface (Fig. 8a) are obviously controlled by the sign of the second derivative of the spectral function with respect to ω at $\omega = 0$. The condition that this second derivative is zero is $\Gamma = \sqrt{3}\Delta_k$. Assuming a simple d-wave gap of the form $\Delta_k = \Delta_0 \cos(2\phi)$ where ϕ is the Fermi surface angle measured relative to the antinode, one then obtains for the position of the arc tip $\phi_0 = 0.5 \cos^{-1}(\Gamma/\sqrt{3}\Delta_0)$. T^* would then be the condition that $\Gamma(T) = \sqrt{3}\Delta_0(T)$.

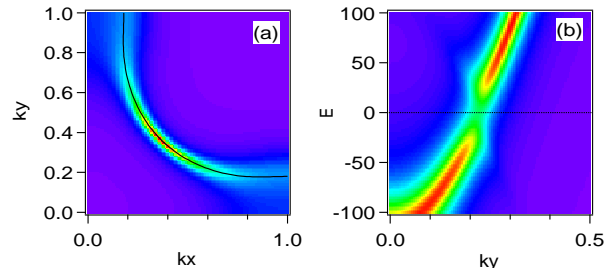


FIG. 7: (Color online) (a) Spectral intensity at zero energy versus k_x, k_y , and (b) versus energy and k_y for $k_x = 0.6$, for the d-wave pair model.

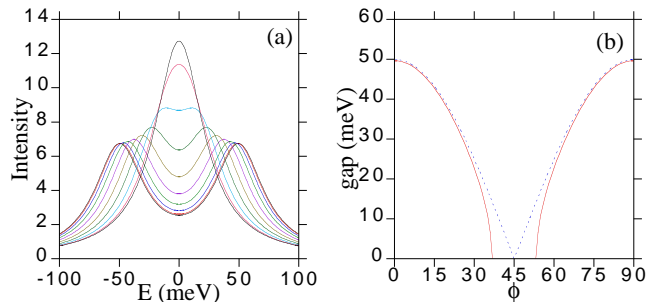


FIG. 8: (Color online) (a) Spectral intensity around the Fermi surface for the d-wave pair model. The top curve is at the node, the bottom curve at the antinode. (b) Spectral gap (half the peak to peak separation) versus the Fermi surface angle. The dashed curve corresponds to $\Gamma=0$.

In Fig. 9a, we show the variation of the arc length with Γ . This variation is consistent with experiment, as shown in Fig. 9a, if one assumes that $\Gamma \propto T$ and Δ_0 is a constant in T (similar plots are shown in Refs. 43,54). This linear variation of the arc length with Γ is a natural consequence of the linear variation of Δ_k with ϕ around the node. The upturn of the arc length at larger Γ is due to the quadratic dependence of the energy gap with ϕ about the antinode.

The theory of Varma and Zhu²⁹ is similar except that Δ_k is taken to be the square of the d-wave gap. As they point out, this fits the angular anisotropy of the parameter Δ_k in the pseudogap phase¹⁶ better than the simple d-wave model, as can be seen in Fig. 9b. On the other hand, the arc length variation with T is more consistent with the simple d-wave form, as shown in Fig. 9a, though we remark that Varma and Zhu were able to obtain a much better fit to the arc length by allowing a self-energy with a more sophisticated frequency and temperature dependence.²⁹

IV. CONCLUSIONS

In regards to the ‘non zero q’ scenarios, there are several ways that experiment could address this question.

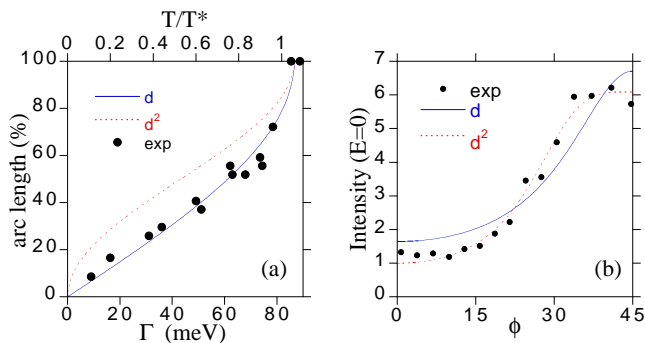


FIG. 9: (Color online) (a) Arc length versus Γ for a d-wave gap and a d^2 gap (data from Ref. 16). (b) Experimental spectral intensity at zero energy versus Fermi surface angle (as in Fig. 2b) versus fits that assume either a d-wave gap ($\cos(2\phi)$) or a d^2 gap ($\cos^2(2\phi)$).

Definitive evidence would be finding a departure of the arc from the underlying normal state Fermi surface, evidence for an energy gap which is asymmetric in energy relative to the chemical potential, or the existence of shadow bands (i.e., bands displaced from the main band by the wavevector q). Other evidence would be the existence of intensity suppression at ‘hot spots’ (where the Fermi surface would cross the Luttinger surface), as has been observed by ARPES in electron doped cuprates.⁵⁵

In regards to the ‘zero q ’ scenarios, the simplest theory consistent with the data appears to be a d-wave gap with an inverse lifetime that is proportional to T . There are, though, some limitations of this model. The data of Ref. 16 were actually fit with a form more general than that of Eq. 9⁵⁶

$$G_k^{-1} = \omega - \epsilon_k + i\Gamma_1 - \frac{\Delta_k^2}{\omega + \epsilon_k + i\Gamma_0} \quad (10)$$

This ‘two lifetime’ model has the advantage of being able to describe a broad spectral function (Γ_1) but with a sharp leading edge gap (Γ_0) as indicated by ARPES data in the pseudogap phase.^{4,6,56} It has since been extended to include a more general frequency dependence for the self-energy.⁵⁷ The presence of two lifetimes may seem unusual, as this does not occur, for instance, in the standard Eliashberg treatment of strong coupling superconductors.⁵⁸ The motivation in Ref. 56 was that Γ_1 denotes the interaction in the particle-hole channel, whereas Γ_0 denotes that in the particle-particle channel. If the dispersion of the single particle states is ignored,

a calculation of fermions interacting with pair fluctuations leads to Γ_0 proportional to $T - T_c$.⁵⁶ In contrast, in two dimensions, a dependence proportional to $\sqrt{T - T_c}$ is obtained.⁵⁹ Consideration of vortex excitations²⁴ leads instead to linear T behavior at high T . In general, one would expect linear T behavior at high temperatures, since this occurs for any model of fermions interacting with bosons,⁶⁰ but with a collapse to zero at T_c since the inverse pair lifetime should vanish in the ordered state. This general T dependence not only naturally describes the linear T variation of the arc length,¹⁶ it can also account for the ‘filling up’ of the gap in the antinodal region.⁵⁶ It also explains why the arc length collapses to zero within the resistive width of the transition.²⁰ Regardless, our experience has been that two lifetimes are necessary to properly model the data.^{16,56,57} A complete description of modeling based on Eq. 10 in regards to the ARPES data is beyond the scope of the present paper and will be left for a future study.

The fits presented in Ref. 16 also indicated that the gap anisotropy changed with temperature, and that this effect could not be described by lifetime broadening of the zero temperature gap, though it should be remarked that the actual value of Δ_k is difficult to extract once the broadening significantly exceeds Δ_k . Whether such changes in anisotropy (and in particular, a region around the node where Δ_k is identically zero as indicated by these fits) can be described by pair breaking within a strong-coupling Eliashberg context remains to be seen. Certainly, careful measurements of the gap anisotropy at different temperatures and dopings would help to better differentiate models based on a d-wave gap from more novel ones, such as that of Varma and Zhu,²⁹ that have a fundamentally different gap anisotropy.

In conclusion, we believe that a model of a d-wave gap with a temperature dependent lifetime consistent with fluctuating pairs gives the simplest description of ARPES data in the pseudogap phase. Future experimental work should be aimed at further differentiating between various proposed models for the Fermi arc, as well as using this information to address other data, such as transport.

Acknowledgments

This work was supported by the U.S. DOE, Office of Science, under Contract No. DE-AC02-06CH11357 and by NSF DMR-0606255.

¹ C. C. Tsuei and J. R. Kirtley, Rev. Mod. Phys. **72**, 969 (2000).

² M.R. Norman, D. Pines and C. Kallin, Adv. Phys. **54**, 715 (2005).

³ D.S. Marshall, D.S. Dessau, A.G. Loeser, C-H. Park, A.Y.

Matsuura, J.N. Eckstein, I. Bozovic, P. Fournier, A. Kapitulnik, W.E. Spicer and Z.-X. Shen, Phys. Rev. Lett. **76**, 4841 (1996).

⁴ H. Ding, T. Yokoya, J. C. Campuzano, T. Takahashi, M. Randeria, M. R. Norman, T. Mochiku, K. Kadowaki and

- J. Giapintzakis, *Nature* **382**, 51 (1996).
- ⁵ A. G. Loeser, Z.-X. Shen, D. S. Dessau, D. S. Marshall, C. H. Park, P. Fournier and A. Kapitulnik, *Science* **273**, 325 (1996).
 - ⁶ M. R. Norman, H. Ding, M. Randeria, J. C. Campuzano, T. Yokoya, T. Takeuchi, T. Takahashi, T. Mochiku, K. Kadowaki, P. Guptasarma and D. G. Hinks, *Nature* **392**, 157 (1998).
 - ⁷ C. C. Homes, T. Timusk, R. Liang, D. A. Bonn and W. N. Hardy, *Phys. Rev. Lett.* **71**, 1645 (1993).
 - ⁸ J. W. Loram, K. A. Mirza, J. R. Cooper, W. Y. Liang and J. M. Wade, *J. Supercond.* **7**, 243 (1994).
 - ⁹ G. Deutscher, *Nature* **397**, 410 (1999).
 - ¹⁰ M. Le Tacon, A. Sacuto, A. Georges, G. Kotliar, Y. Gallais, D. Colson and A. Forget, *Nature Phys.* **2**, 537 (2006).
 - ¹¹ K. Tanaka, W. S. Lee, D. H. Lu, A. Fujimori, T. Fujii, Risdiana, I. Terasaki, D. J. Scalapino, T. P. Devereaux, Z. Hussain and Z.-X. Shen, *Science* **314**, 1910 (2006).
 - ¹² T. Kondo, T. Takeuchi, A. Kaminski, S. Tsuda and S. Shin, *Phys. Rev. Lett.* **98**, 267004 (2007).
 - ¹³ M. C. Boyer, W. D. Wise, K. Chatterjee, M. Yi, T. Kondo, T. Takeuchi, H. Ikuta and E. W. Hudson, arXiv:0705.1731
 - ¹⁴ J. Mesot, M. R. Norman, H. Ding, M. Randeria, J. C. Campuzano, A. Paramekanti, H. M. Fretwell, A. Kaminski, T. Takeuchi, T. Yokoya, T. Sato, T. Takahashi, T. Mochiku and K. Kadowaki, *Phys. Rev. Lett.* **83**, 840 (1999).
 - ¹⁵ M. R. Norman in *High Temperature Superconductivity*, ed. S. E. Barnes, J. Ashkenazi, J. L. Cohn and F. Zuo (American Institute of Physics, 1999), p. 298.
 - ¹⁶ A. Kanigel, M. R. Norman, M. Randeria, U. Chatterjee, S. Souma, A. Kaminski, H. M. Fretwell, S. Rosenkranz, M. Shi, T. Sato, T. Takahashi, Z. Z. Li, H. Raffy, K. Kadowaki, D. Hinks, L. Ozyuzer and J. C. Campuzano, *Nature Physics* **2**, 447 (2006).
 - ¹⁷ J. C. Campuzano, H. Ding, M. R. Norman, H. M. Fretwell, M. Randeria, A. Kaminski, J. Mesot, T. Takeuchi, T. Sato, T. Yokoya, T. Takahashi, K. Kadowaki, P. Guptasarma, D. G. Hinks, Z. Konstantinovic, Z. Z. Li and H. Raffy, *Phys. Rev. Lett.* **83**, 3709 (1999).
 - ¹⁸ N. Doiron-Leyraud, M. Sutherland, S. Y. Li, L. Taillefer, R. Liang, D. A. Bonn and W. H. Hardy, *Phys. Rev. Lett.* **97**, 207001 (2006).
 - ¹⁹ T. Valla, A. V. Federov, J. Lee, J. C. Davis and G. D. Gu, *Science* **314**, 1914 (2006).
 - ²⁰ A. Kanigel, U. Chatterjee, M. Randeria, M. R. Norman, S. Souma, M. Shi, Z. Z. Li, H. Raffy and J. C. Campuzano, unpublished.
 - ²¹ M. Randeria, N. Trivedi, A. Moreo and R. T. Scalettar, *Phys. Rev. Lett.* **69**, 2001 (1992).
 - ²² V. J. Emery and S. A. Kivelson, *Nature* **374**, 434 (1995).
 - ²³ M. Randeria, in *Proceedings of the International School of Physics "Enrico Fermi" Course CXXXVI on High Temperature Superconductors*, ed. G. Iadonisi, J. R. Schrieffer, and M. L. Chialfalo, (IOS Press, 1998), p. 53; cond-mat/9710223.
 - ²⁴ M. Franz and A. J. Millis, *Phys. Rev. B* **58**, 14572 (1998).
 - ²⁵ M. Franz and Z. Tesanovic, *Phys. Rev. Lett.* **87**, 257003 (2001).
 - ²⁶ P. W. Anderson, arXiv:cond-mat/0701042.
 - ²⁷ E. Berg and E. Altman, arXiv:0705.1566.
 - ²⁸ Y. Wang, L. Li and N. P. Ong, *Phys. Rev. B* **73**, 024510 (2006).
 - ²⁹ C. M. Varma and L. Zhu, *Phys. Rev. Lett.* **98**, 177004 (2007).
 - ³⁰ E.-A. Kim, M. J. Lawler, P. Oretto, E. Fradkin and S. A. Kivelson, arXiv:0705.4099.
 - ³¹ X.-G. Wen and P. A. Lee, *Phys. Rev. Lett.* **80**, 2193 (1998).
 - ³² P. A. Lee, N. Nagaosa and X.-G. Wen, *Rev. Mod. Phys.* **78**, 17 (2006).
 - ³³ C. Gros, B. Edegger, V. N. Muthukumar and P. W. Anderson, *Proc. Natl. Acad. Sci.* **103**, 14298 (2006).
 - ³⁴ R. Sensarma, M. Randeria and N. Trivedi, *Phys. Rev. Lett.* **98**, 027004 (2007).
 - ³⁵ A. Paramekanti and E. Zhao, *Phys. Rev. B* **75**, 140507 (2007).
 - ³⁶ A.-M. S. Tremblay, B. Kyung and D. Senechal, *Low Temp. Phys.* **32**, 424 (2006).
 - ³⁷ E. Z. Kuchinski and M. V. Sadovskii, *J. Exp. Theor. Phys.* **103**, 415 (2006).
 - ³⁸ C. Li, S. Zhou and Z. Wang, *Phys. Rev. B* **73**, 060501 (2006).
 - ³⁹ M. Granath, *Phys. Rev. B* **69**, 214433 (2004) and **74**, 245112 (2006).
 - ⁴⁰ S. Chakravarty, R. B. Laughlin, D. K. Morr and C. Nayak, *Phys. Rev. B* **63**, 094503 (2001).
 - ⁴¹ M. Civelli, M. Capone, S. S. Kancharla, O. Parcolet and G. Kotliar, *Phys. Rev. Lett.* **95**, 106402 (2005).
 - ⁴² R. K. Kaul, A. Kolezhuk, M. Levin, S. Sachdev and T. Senthil, *Phys. Rev. B* **75**, 235122 (2007).
 - ⁴³ M. Guidry, Y. Sun and C.-L. Wu, arXiv:0705.0822.
 - ⁴⁴ K.-Y. Yang, T. M. Rice and F.-C. Zhang, *Phys. Rev. B* **73**, 174501 (2006); B. Valenzuela and E. Bascones, *Phys. Rev. Lett.* **98**, 227002 (2007).
 - ⁴⁵ T. Tanescu, P. W. Phillips and T.-P. Choy, *Phys. Rev. B* **75**, 104503 (2007).
 - ⁴⁶ P. Phillips, *Ann. Phys.* **321**, 1634 (2006).
 - ⁴⁷ T. D. Stanescu and G. Kotliar, *Phys. Rev. B* **74**, 125110 (2006).
 - ⁴⁸ A. M. Tsvelik and A. V. Chubukov, *Phys. Rev. Lett.* **98**, 237001 (2007).
 - ⁴⁹ K. McElroy, *Nat. Phys.* **2**, 441 (2006).
 - ⁵⁰ M. R. Norman, M. Randeria, H. Ding and J. C. Campuzano, *Phys. Rev. B* **52**, 615 (1995).
 - ⁵¹ O. Fischer, M. Kugler, I. Maggio-Aprile, C. Berthod and C. Renner, *Rev. Mod. Phys.* **79**, 353 (2007).
 - ⁵² In Bi2212, the only observed shadow bands so far have been of structural origin, due to its orthorhombic unit cell and its superlattice modulation with $q_{SL} = \pi(0.21, 0.21)$. The former has a wavevector of $q_{ortho} = (\pi, \pi)$ which has complicated looking for effects of commensurate antiferromagnetism, flux phases, and d-density waves which have the same characteristic wavevector. For these structural features, though, there is no evidence for an associated energy gap.
 - ⁵³ U. Chatterjee, M. Shi, A. Kaminski, A. Kanigel, H. M. Fretwell, K. Terashima, T. Takahashi, S. Rosenkranz, Z. Z. Li, H. Raffy, A. Santander-Syro, K. Kadowaki, M. R. Norman, M. Randeria and J. C. Campuzano, *Phys. Rev. Lett.* **96**, 107006 (2006).
 - ⁵⁴ J. G. Storey, J. L. Tallon, G. V. M. Williams and J. W. Loram, *Phys. Rev. B* **76**, 060502 (2007).
 - ⁵⁵ N. P. Armitage, D. H. Lu, D. L. Feng, C. Kim, A. Damescelli, K. M. Shen, F. Ronning, Z.-X. Shen, Y. Onose, Y. Taguchi and Y. Tokura, *Phys. Rev. Lett.* **86**, 1126 (2001).
 - ⁵⁶ M. R. Norman, M. Randeria, H. Ding and J. C. Campuzano, *Phys. Rev. B* **57**, R11093 (1998).
 - ⁵⁷ M. R. Norman, A. Kaminski, J. Mesot and J. C. Campuzano, *Phys. Rev. B* **63**, 140508 (2001).

⁵⁸ G. M. Eliashberg, J. Exp. Theor. Phys. **11**, 696 (1960).

⁵⁹ K. Maki and H. Won, Physica C **282-287**, 1839 (1997).

⁶⁰ E. Abrahams, A. V. Chubukov, A. J. Millis and M. R.

Norman, unpublished.